

Optimized control of three-phase inverters to minimize total harmonic distortion in a grid-connected photovoltaic system

Lamreoua Abdelhak^{1,2}, Benslimane Anas², Bouchnaif Jamal¹, El Ouariachi Mostafa^{1,2}

¹Laboratory of Electrical Engineering and Maintenance (LEEM), Higher School of Technology, University of Mohammed I, Oujda, Morocco

²Laboratory Renewable Energy, Embedded System and Information Processing, National School of Applied Sciences, University of Mohammed I, Oujda, Morocco

Article Info

Article history:

Received Feb 16, 2022

Revised Jun 25, 2022

Accepted Jul 17, 2022

Keywords:

Grid

Multi-level inverter

Photovoltaic inverter

Space vector control

Total harmonic distortion

ABSTRACT

Currently, the energy transfer process to the grid of the PV system is based on the importance of less harmonics and high efficiency. The evaluation of harmonics distortion of current is based on the value of THDi ($\ll 5\%$), this last becomes very high if the current leakage is high, which causes losses of the grid and safety problems. Therefore, our job is to improve the classic control method of PV inverters used to reduce grid loss and improve electricity prices. This study is a proposal toward the modelization and improvement of the three-phase two-level, and multi-level photovoltaic (PV) inverter command, using space vector, and sinusoidal control based on controlling the active and reactive current delivered into the grid indirectly with a resonant controller (PIR) for a nonlinear load (NLL). The results of the simulations obtained by the new control methodology, SPWM, and SVPWM show that its performance is better compared with the simple modulation (PWM); the total harmonic distortion (THD) of current in both methods (SVPWM) and (SPWM) is better than that obtained with conventional commands. Also, multilevel converters control produces better quality waveforms, reducing current harmonic distortion.

This is an open access article under the [CC BY-SA](https://creativecommons.org/licenses/by-sa/4.0/) license.



Corresponding Author:

Lamreoua Abdelhak

Laboratory of Electrical Engineering and Maintenance (LEEM)

Higher School of Technology, University of Mohammed I

Boîte Postale 724, Oujda 60000 Oriental, Morocco

Email: a.lamreoua@gmail.com, or lamreoua.abdelhak@ump.ac.ma

1. INTRODUCTION

In recent years, photovoltaic inverters of several types without transformers and with transformers for a multi-control architecture are mainly used to supply electrical energy from the photovoltaic systems to the grid [1]–[3]. Thus, the energy transfer process of the photovoltaic system is based on the importance of good price, small size, and high efficiency [4]–[6]. The harmonic distortion of current (THDi) becomes very high if the current leakage is high, which causes losses of the grid and safety problems for personnel close to the latter [7]–[9]. Different types of full-bridge inverters controlled by the sinusoidal control technique (SPWM) are used for the elimination of these current loss problems [10]–[13]. Therefore, multilevel converters have been considered a preferred topology for large powers due to their advantages such as high levels, overall efficiency, and high output waveform quality [14]–[16]. Against this background, we proposed three-phase and single-phase inverters. These are no longer used to send pure sinusoidal current signals to the grid in phases [17]–[19]. To achieve these goals, the choice of these photovoltaic inverters is based on the equivalence between the reactive power supplied and the nominal power consumed by the grid,

with the cost of these inverters. It is expressed in terms of power related to the quality of the energy supplied to the grid [20], [21]. The integral action (I) of the resonant proportional controller (PR) acts directly on the DC component and guarantees a follow-up of the alternating current. It also eliminates current variations caused by non-linear loads and the non-ideal inverter [22], [23]. Therefore, precise monitoring of the mains voltage vector by a PLL system is necessary to guarantee the proper functioning of our control method [24], [25]. After improving and comparing the various controls of the single-phase inverter [26], [27], this part of the ordered object is about a three-phase PV inverter and a new control method with SVPWM and SPWM control. The latter allows indirect control of currents drawn from the grid by converting these inverter currents into active and reactive powers using three-phase systems. The results obtained with the new control methods SPWM and SVPWM show their performance superior to the simple modulation applied to different levels of inverters in the previous article [28], [29]. After analyzing the simulation results of the control method, it was found that the harmonic distortion of the current under load is much lower than the international standard ($\ll 5\%$) for the two control methods, with a better THD of (SVPWM) compared to that obtained by sine wave control (SPWM). After developing the electrical performance of a three-phase two-stage PV inverter using two different command algorithms under a non-linear load, we have proposed another architecture of multi-level inverters, the latter improves grid performance and provides better waves than a two-level inverter. Multi-level topologies require the use of a large number of semiconductor components to eliminate harmonics and reduce switching losses. Multistage converters produce higher quality waveforms and reduce current and voltage harmonics, thus reducing the current loss caused by high frequencies.

2. PV SYSTEM SCHEME AND MODELING

2.1. Description of our research system and the three-phase photovoltaic inverter

The shape of the proposed three-phase photovoltaic inverter is proven in Figure 1. It includes a PV generator as an energy source, an MPPT block to make certain the tracking of the MPPT, a transistor bridge which includes a current converter provided through the PV generator, and at the end a filter to repel harmonics at excessive frequencies. Topology of three-phase photovoltaic inverter. Figure 2 presents the typical schematic of a three-phase inverter with two levels, here, the phase voltage is expressed by the relationship between the functions of the voltages U and hk:

$$v_{k0} = h_k * \frac{U}{2} \tag{1}$$

$$v_{k0} = \frac{1}{3} \begin{vmatrix} 2 & -1 & -1 \\ -1 & 2 & -1 \\ -1 & -1 & 2 \end{vmatrix} \begin{vmatrix} h1 \\ h2 \\ h3 \end{vmatrix} * \frac{U}{2} \tag{2}$$

The reference voltage \vec{V}_{ref} is expressed by the following expression:

$$(\vec{V}_{ref})_n = (\vec{V})_n = \frac{1}{T_{MLI}} \left\{ \int_0^{T_k} \vec{V}_k dt + \int_0^{T_{k+1}} \vec{V}_{k+1} dt + \int_0^{(1-k)T_0/2} \vec{V}_0 dt + \int_0^{kT_0/2} \vec{V}_7 dt \right\} \tag{3}$$

with $\vec{V}_0 = \vec{V}_7 = \vec{0}$:

$$(\vec{V}_{ref})_n = (\vec{V})_n = \frac{1}{T_e} (T_k \cdot \vec{V}_k + T_{k+1} \cdot \vec{V}_{k+1}) \tag{4}$$

$$T_0 = T_{MLI} - (T_k + T_{k+1}) \tag{5}$$

The voltage vector is null at T0. Therefore, the voltage values for the switch configurations in the diagram (α , β) are presented in Table 1.

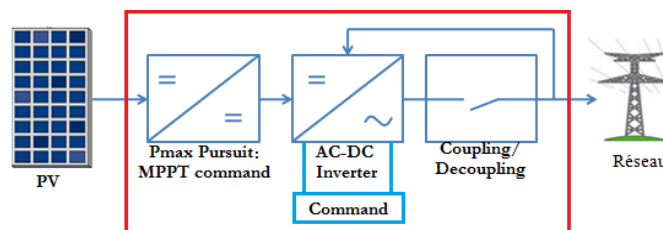


Figure 1. Schematic of photovoltaic inverter with the grid

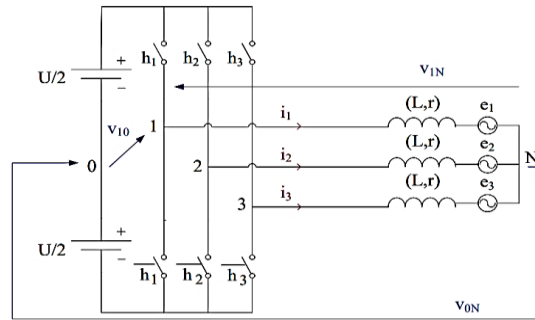


Figure 2. Structure of three-phase inverter

Table 1. Shows the voltage values for the switch configurations in the diagram (α, β)

$h_1h_2h_3$	V_{1n}	V_{2n}	V_{3n}	$V\alpha$	$V\beta$	$\sqrt{Va^2 + V\beta^2}$	Phase ($^\circ$)	V_s	U_{12}
[1-1-1]	2U3	-U3	-U3	$\sqrt{\frac{2}{3}}U$	0	$\sqrt{\frac{2}{3}}U$	0	V1	U
[1 1-1]	U3	U3	-2U3	U6	U2	$\sqrt{\frac{2}{3}}U$	60	V2	0
[-11-1]	-U3	2U3	-U3	-U6	U2	$\sqrt{\frac{2}{3}}U$	120	V3	U
[-1 1 1]	-2U3	U3	U3	$-\sqrt{\frac{2}{3}}U$	0	$\sqrt{\frac{2}{3}}U$	180	V4	-U
[-1-1 1]	-U3	-U3	2U3	-U6	-U2	$\sqrt{\frac{2}{3}}U$	240	V5	0
[1-1 1]	U3	-2U3	U3	U6	-U2	$\sqrt{\frac{2}{3}}U$	300	V6	U
[-1-1-1]	0	0	0	0	0	0	0	V7	0
[1 1 1]	0	0	0	0	0	0	0	V8	0

2.2. Three-phase multi-level inverter

In our case study, we will study only the alternative part AC, the architecture of our system is composed of a PV generator that will be replaced by a voltage source V_{dc} , an interlaced inverter, a LC filter, and the grid. From the Figure 3, we will note that the quantities, V_{i0j} is the voltage vector of cells, V_{inj} is the voltage vector on the inverter side, V_{j2} is the voltage vector, j is the vector of the current injected into the cells of switching of the inverter. q and ijc represent the number of cells, and the current at the capacitor terminal respectively; $ij1$ and $ij2$ are the output currents on the inverter and grid. The subscript j denotes the number of phases ($j = 1, 2, 3$) while i denotes the row of interlaced cells of a phase j ($i = 1, 2, q$). Our system is consisting of a voltage source V_{dc} , an interlaced inverter, a filter, and the grid.

The inverter is controlled by open loop and closed-loop pulse width modulation (MLI). The diagram of the manipulate command of the inverter is proven in Figure 4. The PQ current control unit Figure 5. This part directly controls the output current to the load. This is the same as the total current in the cell. The current loop produces reference voltages U_d^* and U_q^* , which are converted to inverse parks to obtain three sinusoidal voltages at reference ABC. Each current and voltage is used as a reference to be compared to a carrier to generate the control signals MLI at the switches of the inverter. We note that the four carriers are regularly shifted by $T_{sw}/4$ (T_{sw} being the switching period). Note that, the three reference voltages V_x^* are phase-shifted by $2\pi/3$ and the two switches of the same switching cell are complementary $K_i = K_i'$ ($i = 1, 2, 3, 4$ is the cell number).

The three-phase voltage and current are converted to the coordinate dq0 by the Park transformation, as shown in the matrix [L]:

$$\begin{bmatrix} u_d \\ u_q \\ u_0 \end{bmatrix} = [L] \begin{bmatrix} u_A \\ u_B \\ u_C \end{bmatrix} \text{ And } \begin{bmatrix} i_d \\ i_q \\ i_0 \end{bmatrix} = [L] \begin{bmatrix} i_A \\ i_B \\ i_C \end{bmatrix} \text{ with } [L] = \sqrt{\frac{2}{3}} \begin{bmatrix} \sin \alpha & \sin(\alpha - \frac{2\pi}{3}) & \sin(\alpha + \frac{2\pi}{3}) \\ \cos \alpha & \cos(\alpha - \frac{2\pi}{3}) & \cos(\alpha + \frac{2\pi}{3}) \\ \frac{1}{\sqrt{2}} & \frac{1}{\sqrt{2}} & \frac{1}{\sqrt{2}} \end{bmatrix} \quad (6)$$

The reference currents $I^* d$ and $I^* q$ for the line axis can be obtained from the following relationship:

$$\begin{aligned} P &= V_d I_d + V_q I_q \xrightarrow{V_q=0} I^*_d = \frac{P^*}{V_d} \\ Q &= V_d I_q - V_q I_d \xrightarrow{V_q=0} I^*_q = \frac{Q^*}{V_d} \end{aligned} \tag{7}$$

The active (P) and reactive (Q) powers are calculated from the relationships below, with P^* and Q^* being the reference powers:

$$\begin{aligned} P &= V_d I_d \\ Q &= V_d I_q \end{aligned} \tag{8}$$

The reference current $I^* d$ is determined from the dynamic analysis of the capacitor when the power Q is set to zero:

$$\frac{d}{dt} V^2_{DC} = \frac{2}{C} (P_{in} - P_{out}) \tag{9}$$

By application of PI controller on the difference between the output and input power, allows to extract the current reference I^*_d :

$$I^*_d = \frac{1}{V_d} (k_p (P_{in} - P_{out}) + K_I \int (P_{in} - P_{out}) dt) \tag{10}$$

Based on the previous results, we determine the control voltages V^*d and V^*q :

$$\begin{aligned} V^*_d &= k_p (I^*_d - I_q) + K_I \int (I^*_d - I_q) dt - \omega L_f I_d + V_d \\ V^*_q &= k_p (I^*_q - I_q) + K_I \int (I^*_q - I_q) dt - \omega L_f I_q + V_d \end{aligned} \tag{11}$$

in general, our control system is based on the DQ method, and related to PI controllers by the (12).

$$G_{PI}^{(dq)}(s) = \begin{bmatrix} K_p + \frac{K_i}{s} & 0 \\ 0 & K_p + \frac{K_i}{s} \end{bmatrix} \tag{12}$$

Transport delay based PLL structure. The principle of PLL is to use a PI controller to reduce the phase difference between the line phase angle and the voltage output phase angle to zero Figure 6. The Table 2 shows the system parameters during the simulation.

Table 2. Simulation Parameters

PV Power	500 W
V_d	80 V
I_{min}	1 A
f_g	50 Hz
f_{pwm}	10 KHz

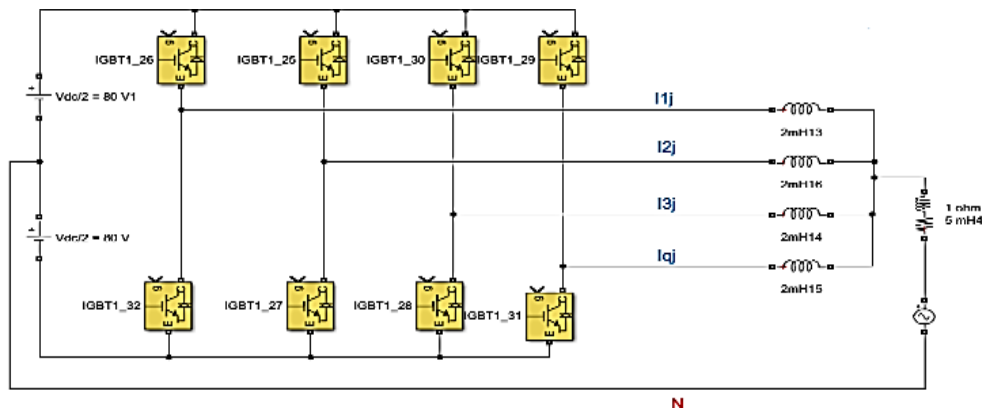


Figure 3. PV grid-connected multi-level inverter (one phase)

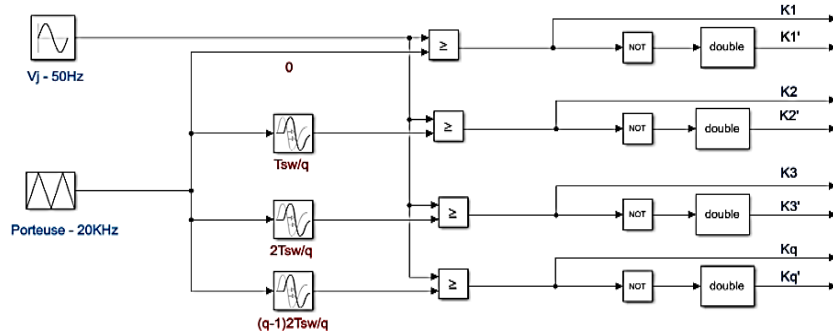


Figure 4. Interlaced inverter SPWM control diagram

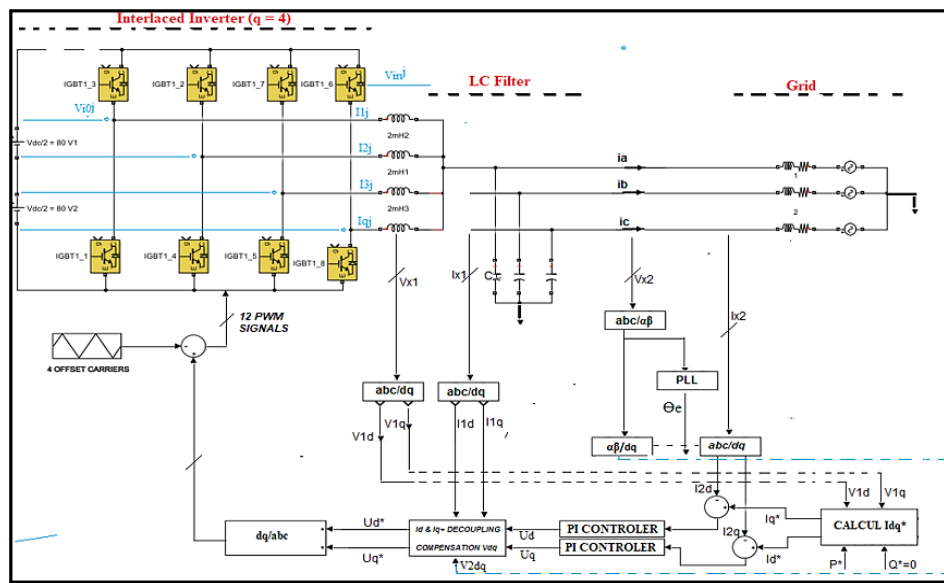


Figure 5. Block illustration of the proposed control system

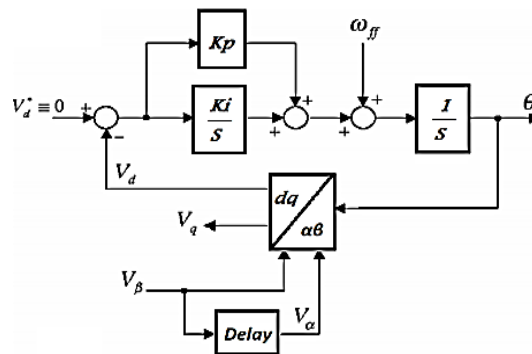


Figure 6. Phase locked loop algorithm

3. SIMULATION RESULTS

3.1. Comparison of the different commands of single-phase photovoltaic inverter

3.1.1. Indirect control by PWM

a. Control by PWM (sine-bipolar triangle)

After analyzing the current spectrum in Figure 7, a signal with near zero harmonics was obtained. This shows that the current THD is 6.31%. On the other hand, we can notice the voltage signal spectrum contains several harmonics, far from the fundamental wave with a current THD of 145.93%.

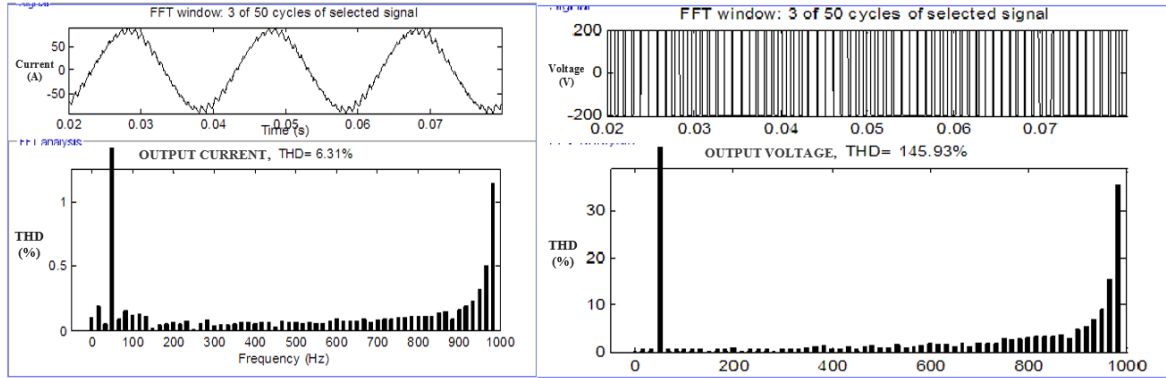


Figure 7. Output current and voltage

b. Control through PWM sine-unipolar triangle (PWM inter-selective)

The current sign received in discern eleven affords much fewer ripples with a quasi-sine wave. On the opposite hand, the voltage of the burden received is variable among values one wonderful 100 V and negative -100V. The discern received from Figure 8 is somewhat sinusoidal, that is proven through a discounted harmonic distortion price same to $THD_i=2.68\%$. The sign of the voltage on the output of the inverter is right however wealthy in excessive frequency harmonics with a voltage THD_v same to: 78.76% .

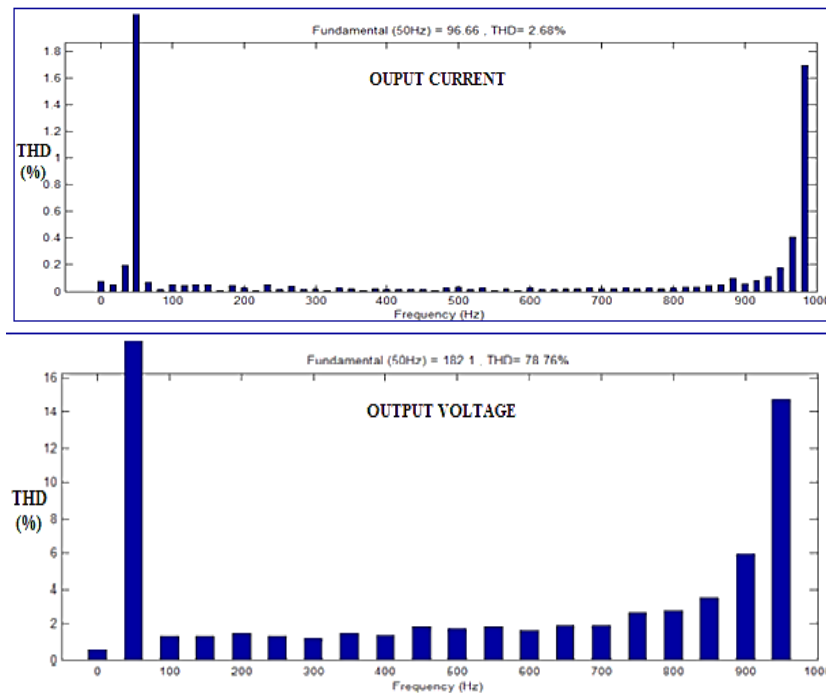


Figure 8. Output current and voltage spectrum

c. Control through the PWM sinus triangle in a closed loop with PI controller

The Proportional Integral controller is represented through the subsequent transfer function:

$$G(s) = Kp + \frac{Ki}{s} \tag{13}$$

the current and the voltage on the terminal of the load in the Figure 9 are solely sinusoidal. The spectral evaluation offers a totally decreased fee of the current THD and the voltage, effectively same $THD_i=0.14\%$ and $THD_v=1.59\%$ decrease than the worldwide standard ($\ll 5\%$). These effects display the vital position of the utility of the PI regulator in a closed loop, which permits to ameliorate of the traits of the system below non-linear load conditions.

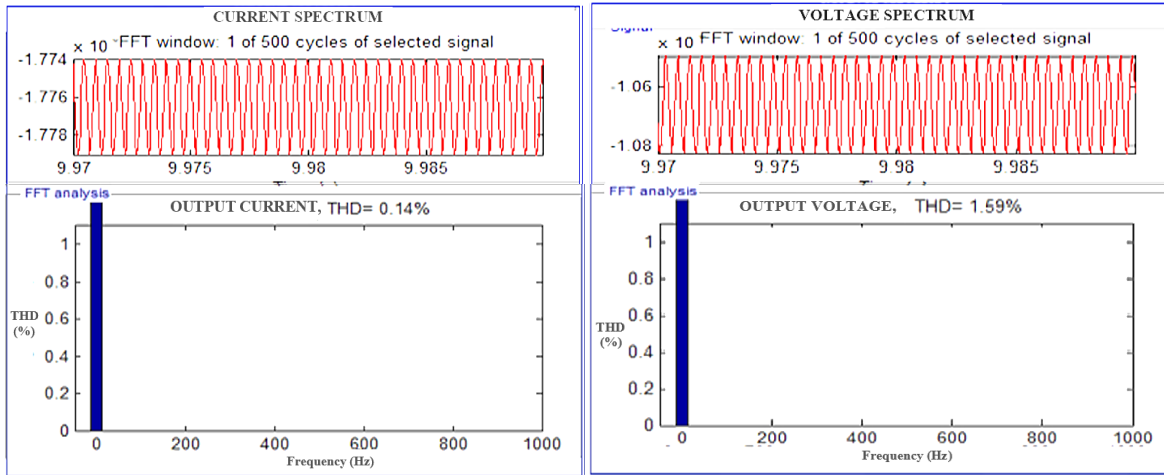


Figure 9. Output current and voltage with pi controller in closed loop

3.1.2. Control by hysteresis

According to the frequency evaluation of the consequences acquired, we observe that the spectrum of current and, of the voltage are barely higher than that acquired through the modulation with a THD identical successively 4.67% and 49.12% for the current and the voltage in the Figure 10. This indicates that this command offers mesh generator consequences and that the hysteresis band is functioning correctly, with harmonics performing at low frequencies.

The results in Table 3 conclude that indirect control with MLI imposes an average phase voltage V at a constant switching frequency, but the dynamic response can be limited by the presence of a resolver. Their advantage is that they push the harmonics of the output voltage too high frequencies. This makes filtering easier (easier to implement and cheaper) and allows you to adjust the amplitude of the fundamental wave of the output voltage. Direct control by hysteresis imposes a non-constant switching frequency on the arm state but has a faster transient response than indirect control due to the absence of a spell leads.

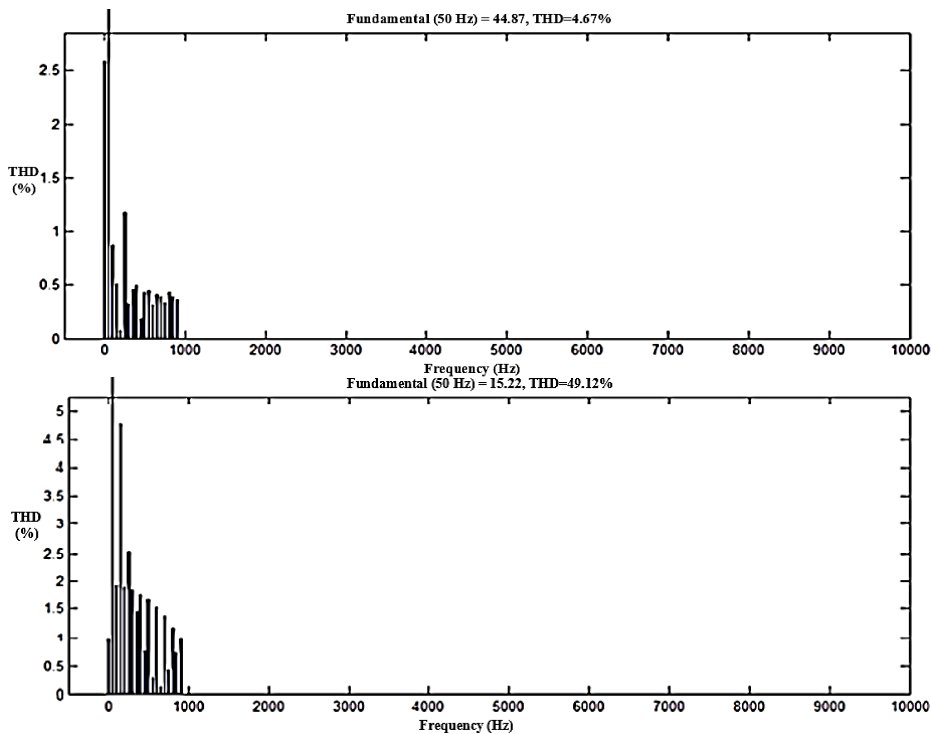


Figure 10. Spectrum of output current and voltage for hysteresis control

Table 3. Comparison of THD for different control method

f	Indirect control by PWM			Direct control by Hysteresis
	PWM sine-bipolar triangle	PWM sine-unipolar triangle	PWM sinus-triangle in closed loop with PI controller	
THD _i	6.31 %	2.68 %	0.14%	4.67%
THD _v	78.76 %	145.93 %	1.59%	49.12%

3.2. A three-phase two-level PV inverter

3.2.1. Sinusoidal PWM control case (SPWM)

After recalling the operating principle of the SPWM and SVPWM command, we will model it under the environment of the MATLAB / SIMULINK software, as shown in the Figure 11. Before filtering: When the three-phase converter is related to the non-linear load (NLL) lead to quality result in great troubles of the energy deliver to the grid. that's proven through the current spectrum of Figure 12 which produces a current signal present odd harmonics of a couple of order, with THD consecutively same to 4, 40% and 4.47% for the current and the voltage.

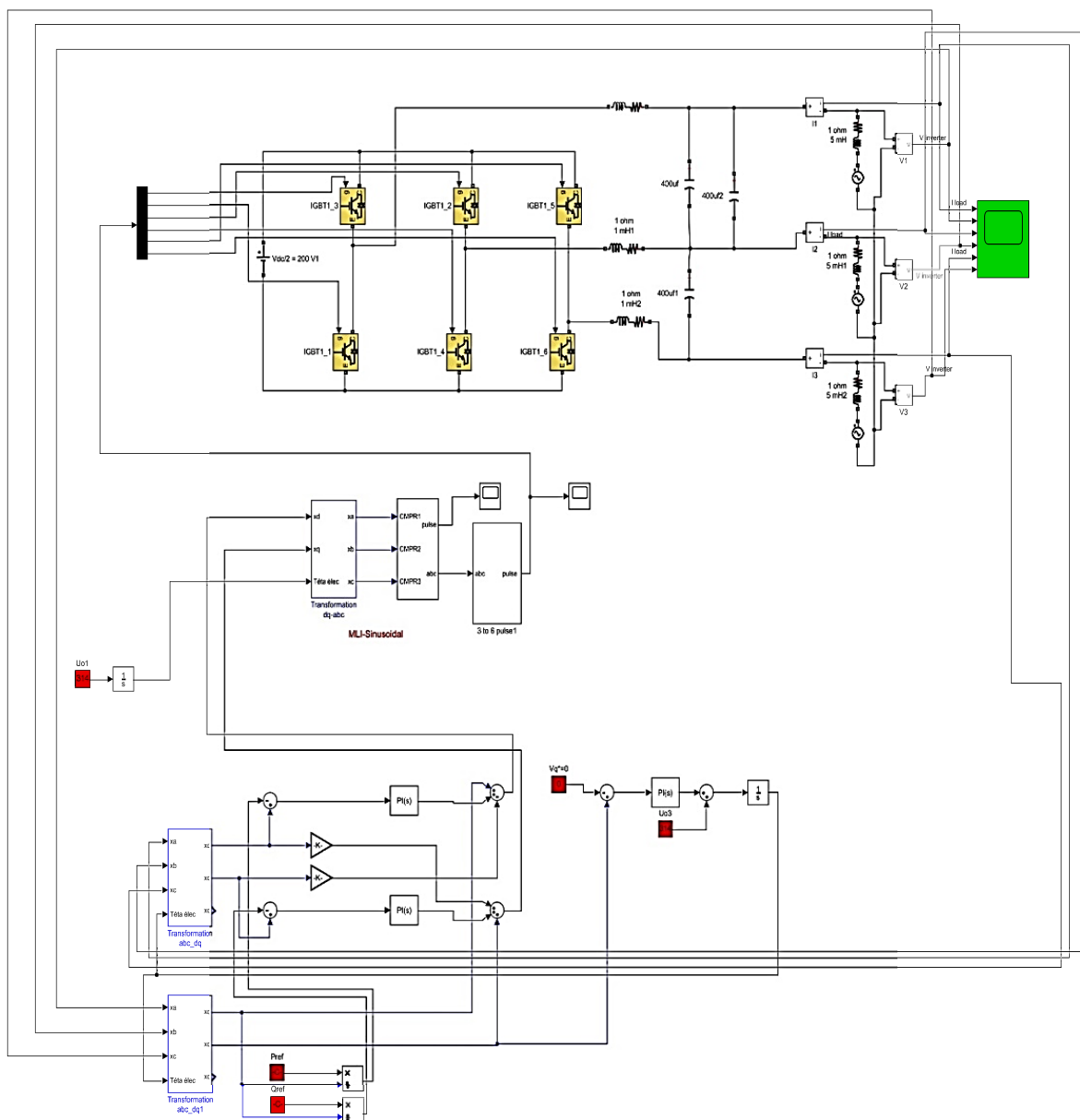


Figure 11. Current control diagram proposed by space vector control (SVPWM) of three-phase PV inverter

With filtering. From the spectral evaluation of Figure13 we be aware that the harmonic distortion rate is decreased and to the norm (lower <5%) with THD same to 0.68% for the current for the voltage 0.05%. what allowed us to obtain a purely sinusoidal signal (variable frequency and amplitude)), furthermore all of the harmonics of the excessive frequencies disappeared afterwards. Therefore, the proposed control allowed us to boom the overall performance on the output of the inverter.

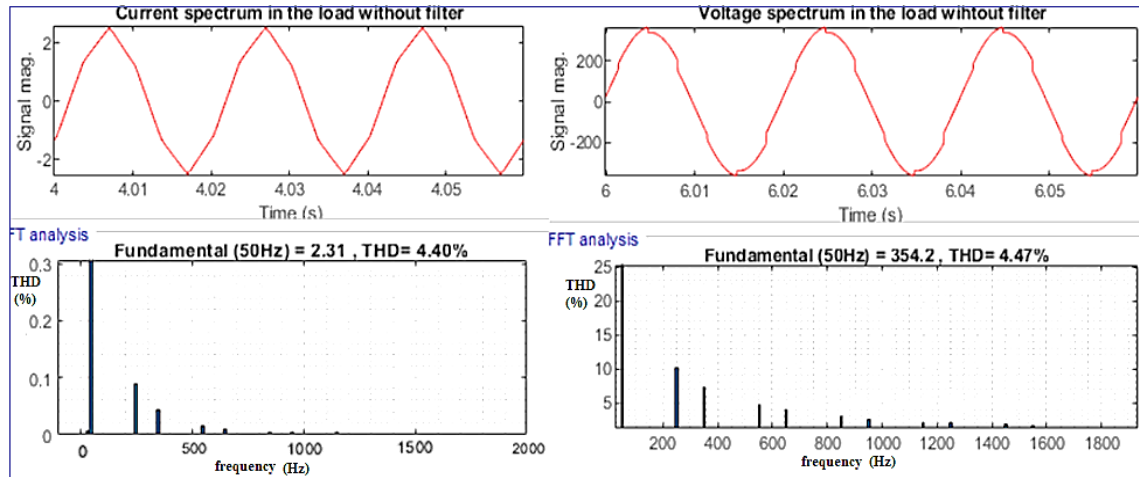


Figure 12. Output FFT of voltage and current before filtering

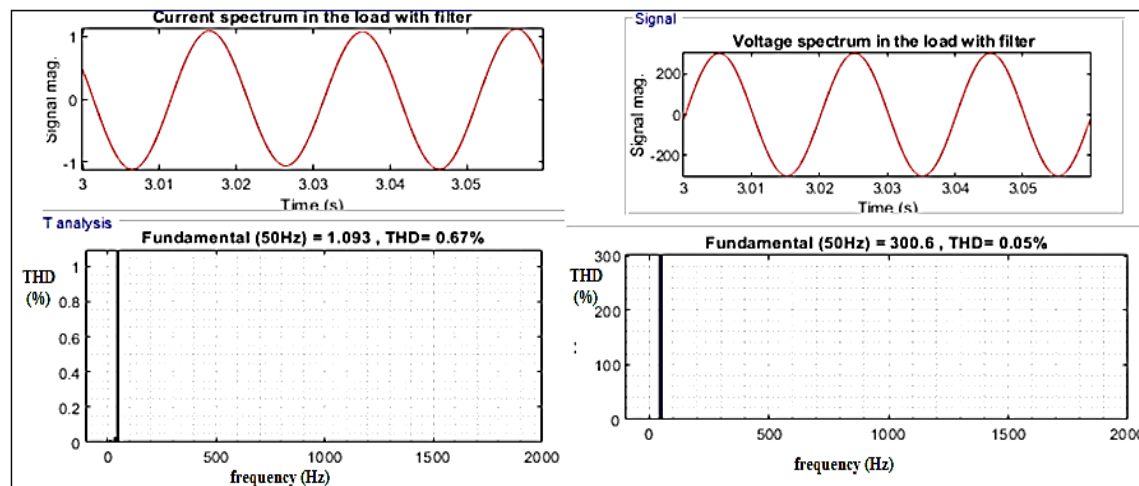


Figure 13. Output FFT of voltage and current after filtering

3.2.2. Space vector control case (SVPWM)

Before filtering. The signal in Figure 14 suggests the shape of current and the output voltage, with a fundamental whose traits are near to the references, the total harmonic distortion rate is same to 4.39% for current, and 4.47% for voltage; which suggests that the presence of significant harmonics, with traits near to that of the very high carrier but easy to filter out. With filtering. The spectral analysis of the Figure 15 presents the results of the simulation after filtering, with a better THD equal successively for current and voltage, 0.22% and 0.04% <<3% (international standards), which shows that the proposed control works correctly and the harmonics of the high frequencies are totally filtered out with an output current signal is purely sinusoidal.

Power variation: the Figure 16 shows the comparative waveforms of active and reactive power in the load and their references after compensation. According to Figure 16 the power (Pa) has an average value equal to the power reference (Pref=500 w) and the power (Qr) is very close to the zero value (Qref=0 kV), after the application of the two controls.

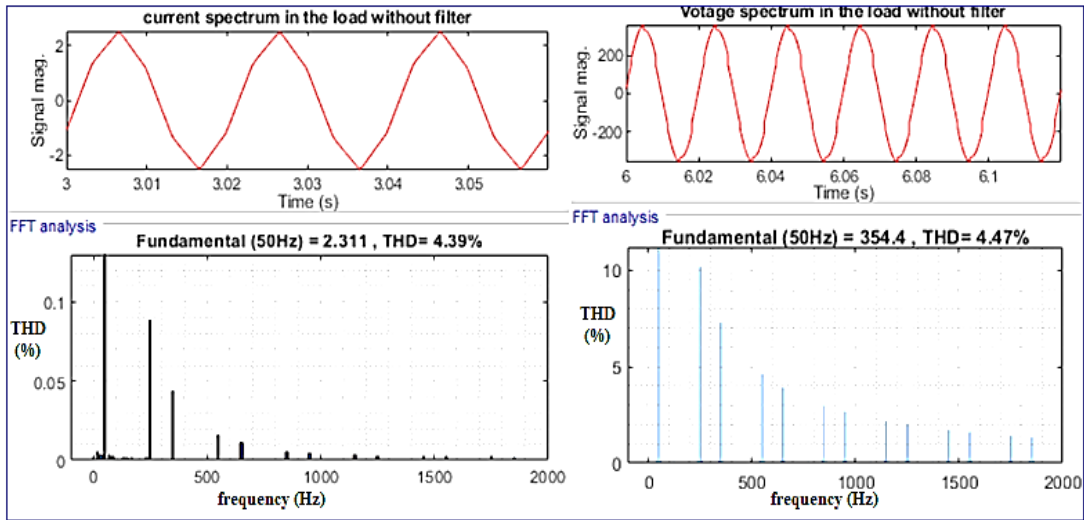


Figure 14. Output FFT of voltage and current before filtering

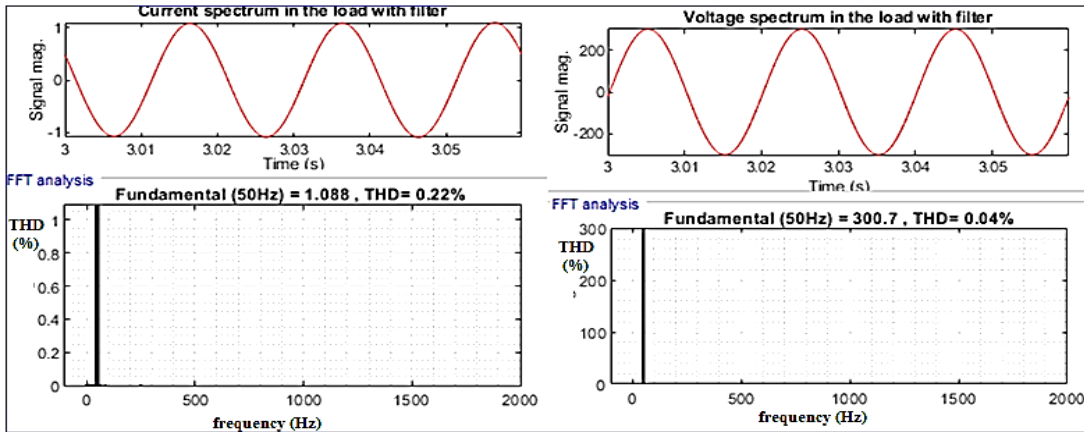


Figure 15. Output FFT of voltage and current with filtering

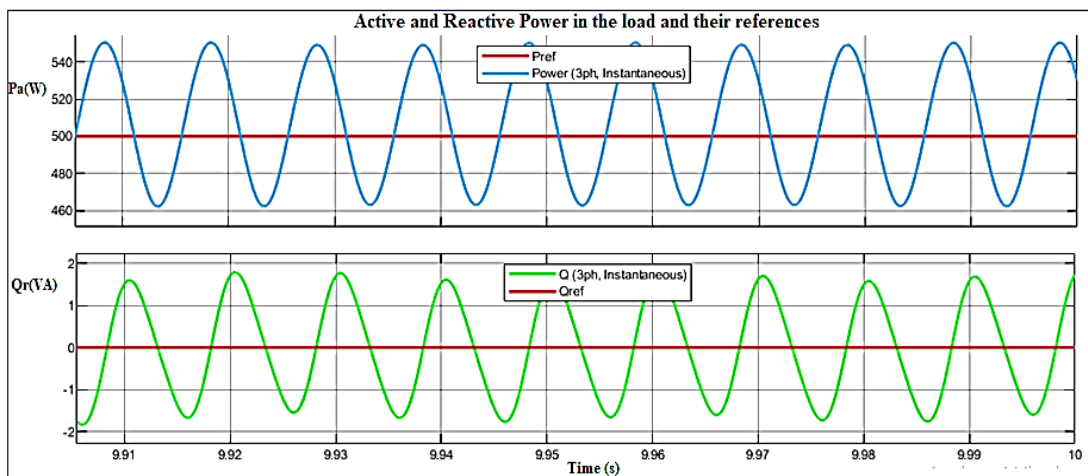


Figure 16. Variation of poer auhtor of their references

3.3. Three-phase multi-level interlaced PV inverter
3.3.1. SPWM control

Figures 17 and 18 show the converter's current and voltage spectra before and after filtering, respectively. It can be seen that the difference in the waveform at the output of the inverter voltage is completely sinusoidal after filtering, but not before filtering. Figure 18 shows the current THD at the converter's input line after filtering. Current and voltage THD for the first harmonic of 50, in contrast to the THD indicator (4.66% and 2.59%), which was acquired by the system before filtering, and the system indicator THD. 0.28% and THDv=0.30%. It is much better to use an interlaced inverter after filtering.

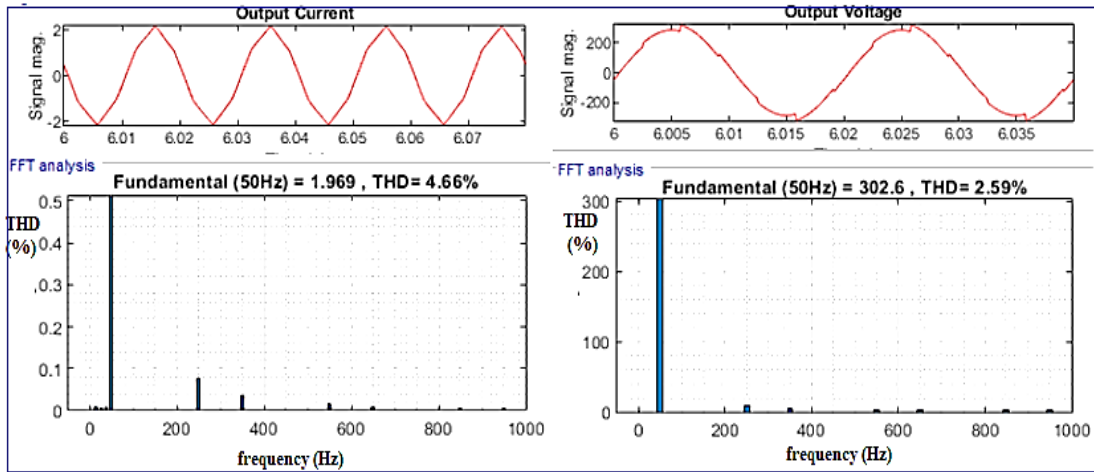


Figure 17. Current and voltage spectra by (SPWM) before filtering

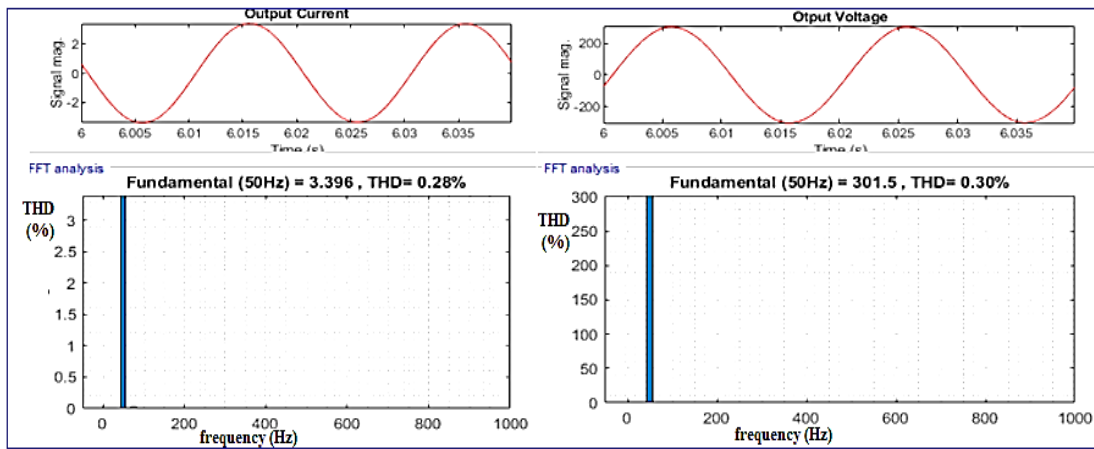


Figure 18. Current and voltage spectra by (SPWM) after filtering

3.3.2. SVPWM control

The THD values obtained at the output of the interlaced inverter are better than those obtained with the classic inverter as shown in the Figures 19 and 20. We also note the improvement in the transient regime of the curves obtained with the interwoven inverter system after filtering compared to the transient regime of the curves of the system with a conventional inverter (THDi = 0.14% and THDv = 0.03) represents the best THD value obtained. Table 4 shows the results obtained after application of the two new control methods by SVPWM and SPWM before and after compensation. Moreover, the values of TDH <<5% with honey rate for the multi-level inverters compared the two-level inverters, which shows that the proposed method are very efficient and solve the problems encountered with the classic three-phase PV inverters.

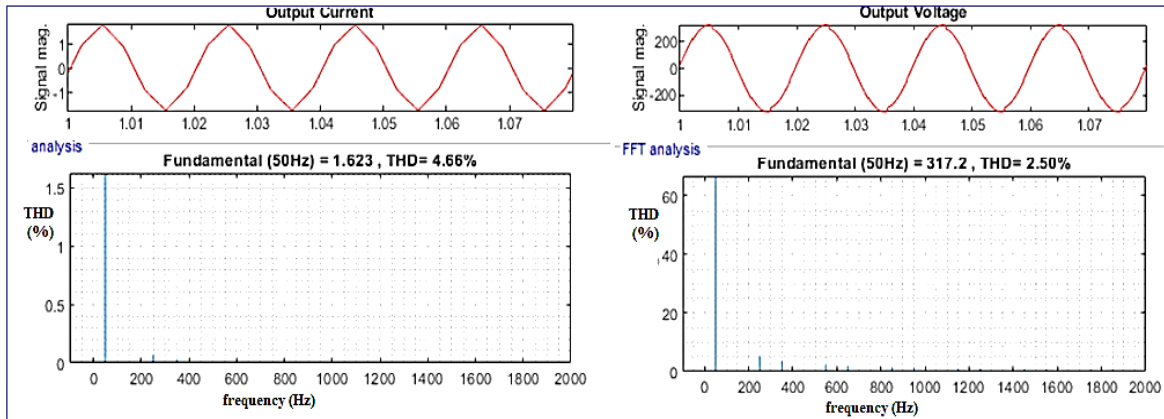


Figure 19. Current and voltage spectra by (SVPWM) before filtering

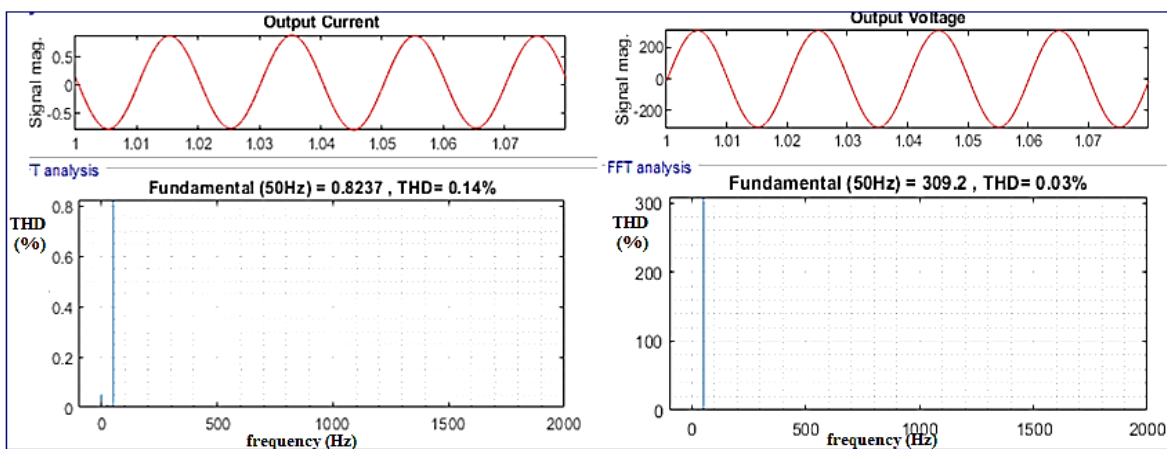


Figure 20. Current and voltage spectra by (SVPWM) before filtering

Table 4. THD of these two typologies

Topology		THD _i		THD _v	
		SPWM	SVPWM	SPWM	SV PWM
Before filtering	Two-level Three-phase PV inverter	4.40%	4.39%	4.47%	4.47%
After filtering		0.67%	0.22%	0.05%	0.04%
Before filtering	Multi-level three phase PV inverter	4.66%	4.66%	2.50%	2.50%
After filtering		0.28%	0.14%	0.30%	0.03%

4. CONCLUSION

In this article, we have compared and improved the electrical characteristics of Three-phase two- and multi-level PV inverter related to the nonlinear load through different control methods, to improve the problems of current harmonics injected into the grid by an inverter related to the PV system. So, in this part, we've modeled the three-phase photovoltaic multi-level inverter, and applied two improved controls of these, via the SVPWM control and SPWM control applied to the non-linear load. From the simulation results, and the spectral evaluation we stated that it has improved the performance of the two control strategies proposed and that the SVPWM (THDi=0.22%) command provides load current characteristics higher than the ones acquired with the SPWM (THDi=0.67%) command. On the other hand, if the inverter levels are increased (case of the interlaced inverter), The performance of the multi-level 3-phase PV inverter is superior to that of the 3-phase 2-level PV inverter, and significant improvements have been seen in the transition state and waveform. with a lower distortion harmonic of current THDi= 0.14%(SVPWM) and THDi=0.28%(SPWM), it is reduced conduction losses, both comply with international standards (<<5%) which shows the efficiency of this control method used and ensures the risk of current leaked injected into the grid.

REFERENCES

- [1] S. Dabbi, A. Aziz, A. Messaoudi, M. El Ouariachi, and I. Mazozi, "Implementation of a multi-control architecture in a photovoltaic/grid/electrolysis system for usual use and clean storage by hydrogen production," *International Journal of Renewable Energy Research (IJRER)*, vol. 7, no. 4, pp.1827-1835, Dec. 2017, doi: 10.20508/ijrer.v7i4.6275.g7226.
- [2] P. S. Subudhi and S. Krithiga, "PV and grid interfaced plug-in EV battery charger operating in P-VG, P-V and V-G modes," *International Journal of Recent Technology and Engineering (IJRTE)*, vol. 8, no. 2, pp. 3431-3443, July 2019, doi: 10.35940/ijrte.B2680.078219.
- [3] A. Mukherjee, S. Krithiga, and P. S. Subudhi, "Investigation of a PV fed improved smart home EV battery charging system using multi output hybrid converter, use and clean storage by hydrogen production," *International Journal of Renewable Energy Research (IJRER)*, vol. 9, no. 2, pp. 392-703, June 2019, doi: 10.20508/ijrer.v9i2.9124.g7639.
- [4] E. Babaei, S. Alilu and S. Laali, "A new general topology for cascaded multilevel inverters with reduced number of components based on developed h-bridge," *IEEE Transactions on Industrial Electronics*, vol. 61, no. 8, pp. 3932-3939, Aug. 2014, doi: 10.1109/TIE.2013.2286561.
- [5] A. Hassan, X. Yang, W. Chen, and M. A. Houran, "A state of the art of the multilevel inverters with reduced count component," *Electronics 2020*, vol. 9, no. 11, Nov. 2020, doi: 10.3390/electronics9111924.
- [6] V. M. Deshmukh and A. J. Patil, "Comparison and performance analysis of closed loop controlled nonlinear system connected PWM Inverter based on hybrid technique," *Journal of Electrical Systems and Information Technology*, vol. 2, no. 1, pp. 86-98, May 2015, doi: 10.1016/j.jesit.2015.03.008.
- [7] Z. Ahmad and S. N. Singh, "Single phase transformerless inverter topology with reduced leakage current for grid connected photovoltaic system," *Electric Power Systems Research*, vol. 154, pp. 193-203, Jan. 2018, doi: 10.1109/TPEL.2018.2886054.
- [8] E. Babaei and E. Shokati Asl, "A new topology for Z-source half bridge inverter with low voltage stress on capacitors," *Electric Power Systems Research*, vol. 140, pp. 722-734, Nov. 2016, doi: 10.1016/j.epr.2016.04.010.
- [9] D. Stojic, T. Traczewski, and I. Klasnic, "Proportional-integral-resonant AC current controller," *Advances in Electrical and Computer Engineering*, vol. 17, no. 1, Feb. 2017. Energies 2021, doi: 10.3390/en14206726.
- [10] M. Karimi, M. R. J. Oskuee, S. N. Ravadanegh, and G. B. Gharehpetian, "A developed single-phase cascaded multilevel inverter with reduced number of circuit devices," *International Journal of Ambient Energy*, vol. 40, no. 3, pp. 254-262, Oct. 2017, doi: 10.1080/01430750.2017.1372812.
- [11] S. M. Silva, B. M. Lopes, B. J. C. Filho, R. P. Campana and W. C. Bosventura, "Performance evaluation of PLL algorithms for single-phase grid-connected systems," in *Conference Record of the IEEE Industry Applications Conference*, 2004. 39th IAS Annual Meeting., 2004, pp. 2259-2263 vol.4, doi: 10.1109/IAS.2004.1348790.
- [12] N. Golovanov, G. C. Lazaroiu, M. Roscia, and D.Zaninelli. "Power quality assessment in small scale renewable energy sources supplying distribution systems," *Energies*; vol. 6, no. 2, pp. 634-645, doi:10.3390/en6020634.
- [13] Q. -N. Trinh and H. -H. Lee, "An Enhanced Grid Current Compensator for Grid-Connected Distributed Generation Under Nonlinear Loads and Grid Voltage Distortions," *IEEE Transactions on Industrial Electronics*, vol. 61, no. 12, pp. 6528-6537, Dec. 2014, doi: 10.1109/TIE.2014.2320218.
- [14] T. I. Maris, St. Kourtesi, L. Ekonomou, and G.P. Fotis, "Modeling of a single-phase photovoltaic inverter," *Solar Energy Materials and Solar Cells*, vol. 91, no. 18, pp. 1713-1725, Nov. 2007, doi: 10.1016/j.solmat.2007.05.027.
- [15] S. Fernandez, "Commande par hystérésis Modulation d'impulsions en durée Onduleurs Productivité Énergie-Conversion directe," Physics, Thèse Lille, 2013.
- [16] P. Kakosimos, K. Pavlou, A. Kladas, and S Manias, "A single-phase nine-level inverter for renewable energy systems employing model predictive control," *Energy Conversion and Management*, vol. 89, pp. 427-437, Jan. 2015, doi: https://doi.org/10.1016/j.enconman.2014.10.013.
- [17] Y. Yang, F. Blaabjerg and H. Wang, "Low-Voltage Ride-Through of Single-Phase Transformerless Photovoltaic Inverters," in *IEEE Transactions on Industry Applications*, vol. 50, no. 3, pp. 1942-1952, May 2014, doi: 10.1109/TIA.2013.2282966.
- [18] M.R. Bengourina, "Direct power control of a grid connected photovoltaic system, associated with an active power filter;" *Journal of Renewable Energies*, vol. 20, no. 1, pp. 99-109, Mar. 2017, doi: 10.54966/jgreen.v20i1.613.
- [19] A. Naderipour, A. A. Mohd. Zin, M. H. B. Habibuddin, M. r. Miveh, and J. M. Guerrero, "An improved synchronous reference frame current control strategy for a photovoltaic grid-connected inverter under unbalanced and nonlinear load conditions," *Journal Pone*, Feb. 2017, doi: 10.1371/journal.pone.0164856.
- [20] C. Mahamat, "Analyse et commandes des convertisseurs multi-niveaux pour un générateur photovoltaïque connecté au réseau électrique," These, Energie électrique. Université Paris Saclay 2018. Français. ffNNT: 2018SACLN024.
- [21] M. M. Hasan, A. Abu-Siada, and Md. R. Islam, "Design and implementation of a novel three-phase cascaded half-bridge inverter," *IET Power Electronics*, vol. 9, no. 8, pp. 1741-1752, Mar. 2016, doi: 10.1049/iet-pel.2015.0951.
- [22] A. M. Noman, K. E. Addoweesh, A. A. Alabduljabbar, and A. I. Alolah, "Cascaded H-Bridge MLI and Three-Phase Cascaded VSI Topologies for Grid-Connected PV Systems with Distributed MPPT," *International Journal of Photoenergy*, Jan. 2019, doi: 10.1155/2019/7642919.
- [23] T. -F. Wu, C. -H. Chang, L. -C. Lin, G. -R. Yu and Y. -R. Chang, "A D- Σ Digital Control for Three-Phase Inverter to Achieve Active and Reactive Power Injection," *IEEE Transactions on Industrial Electronics*, vol. 61, no. 8, pp. 3879-3890, Aug. 2014, doi: 10.1109/TIE.2013.2286574.
- [24] S. D. V. R. Vadlamudi, D. Jiani, M. A. C. Acosta, C. Shuyu, V. B. Sriram and A. Tripathi, "Decoupled DQ-PLL with positive sequence voltage normalization for wind turbine LVRT control," in *Asian Conference on Energy, Power and Transportation Electrification (ACEPT)*, 2016, pp. 1-6, doi: 10.1109/ACEPT.2016.7811527.
- [25] L. Abdelhak, B. Anas, M. Abdelhafid, A. Aziz, and M. El Ouariachi, "Comparison of the different commands direct and indirect of a single-phase in-verter for Photovoltaic," *International Conference on Electronic Engineering and Renewable Energy (ICEERE)*, vol. 519, Aug. 2018 doi: 10.1007/978-981-13-1405-6_66.
- [26] L. Abdelhak, B. Anas, B. Jamal, and E. Mustofa, "An improved sinusoidal (PWM) and vector (SVPWM) current control for a three-phase photovoltaic inverter connected to a non-linear load," *International Conference on Electronic Engineering and Renewable Energy ICEERE*, Aug. 2020, vol. 681, pp. 481-494, doi: 10.1007/978-981-15-6259-4_51.
- [27] S. Dedeoglu and G. C. Konstantopoulos, "Three-phase grid-connected inverters equipped with nonlinear current-limiting control," *International Conference on Control (CONTROL)*, 2018, pp. 38-43, doi: 10.1109/CONTROL.2018.8516764.
- [28] A. Jura, P. Roncero-Sánchez, A. Mahamadou, E. J. Molina-Martínez, and G. Lefebvre, "HRES power generation: the power injection control and the grid synchronization cases," *International Journal of Renewable Energy Research (IJRER)*, vol 9, no. 2, Jun. 2019, doi: 10.20508/ijrer.v9i2.9050.g7634.

- [29] P. Vu, V. N. Trang, M. N. Dinh, T. N. Cuong, and D. T. Anh, "Modified space vector modulation technique for three phase three level 1-type inverter," *International Journal of Renewable Energy Research (IJRER)*, vol. 11, no. 3, Sep. 2021, doi: 10.20508/ijrer.v11i3.12058.g8256.

BIOGRAPHIES OF AUTHORS



Lamreoua Abdelhak    received the Master. degree in electrical engineering from faculty of science and technology, Cady Ayad University, Marrakech, in 2012 and professional degree in electrical engineering and industrial electronics. degrees from Faculty of Sciences, Cady Ayad University, Marrakech, 2009 is a PhD Researcher a Laboratory of Electrical Engineering and Maintenance (LEEM), Higher School of Technology, University of Mohammed I, Oujda, Morocco. His research interests include the field of industrial informatics, power electronics, motor drives, renewable energy, artificial intelligence, intelligent control. He can be contacted at email: andelhak.lamreoua@ump.ac.ma.



Bouchnaif Jamal    is a Director of Electrical Engineering and Maintenance Laboratory LEEM, Research Professor (PES) at the Higher School of Technology and member of the laboratory of Electrical engineering, power electronics and automotive technology, He is a coordinator of the professional bachelor's degree in industrial maintenance. His research interests include the, industrial applications, industrial electronics, industrial informatics, power electronics, motor drives, renewable energy, Dspace applications, and artificial intelligence. He can be contacted at email: j.bouchnaif@ump.ac.ma.



Anas Benslimane    is associate professor at National school of applied science, Mohammed first university. Oujda. Morocco. He received the State engineer's degree in industrial engineering from National school of applied science Oujda. He holds the Phd degrees in electrical engineering from mohammed first university. His research areas are FACTS devices and power grids. he is a reviewer in some conferences. He can be contacted at email: a.benslimane@ump.ac.ma.



El Ouariachi Mostafa    is a member of the Laboratory of Electrical Engineering and Maintenance LGEM, Professor (PA) at the Higher school of Technology and Member of the laboratory of Photovoltaic Solar Energy and Applications. He is a teaching of the DUT sector in electrical engineering and industrial maintenance at the higher school of technology, university moamed first oujda. His research interests include renewable energy, power quality, power electronics, power grids, relay protection, battery chargers, and harmonic distortion. He can be contacted at email: m.elouariachi@ump.ac.ma.